

On-the-Fly Simulation of Two-Dimensional Fluorescence-Excitation Spectra

Sebastian V. Pios,[†] Maxim F. Gelin,[‡] Luis Vasquez,[‡] Jürgen Hauer,[¶] and Lipeng
Chen^{*,†}

[†]*Zhejiang Laboratory, Hangzhou 311100, China*

[‡]*School of Science, Hangzhou Dianzi University, Hangzhou 310018, China*

[¶]*Department of Chemistry, Technical University of Munich, D-85747 Garching, Germany*

E-mail: chenlp@zhejianglab.com

Abstract

Two-dimensional (2D) fluorescence-excitation (2D-FLEX) spectroscopy is a recently proposed nonlinear femtosecond technique for the detection of photoinduced dynamics. The method records a time-resolved fluorescence signal in its excitation- and detection-frequency dependence, and hence combines the exclusive detection of excited state dynamics (fluorescence) with signals resolved in both excitation and emission frequencies (2D electronic spectroscopy). In this work, we develop an on-the-fly protocol for the simulation of 2D-FLEX spectra of molecular systems, which is based on interfacing the classical doorway-window representation of spectroscopic responses with trajectory surface hopping simulations. Applying this methodology to the gas-phase pyrazine, we show that femtosecond 2D-FLEX spectra can deliver detailed information otherwise obtainable via attosecond spectroscopy.

Two-dimensional electronic spectroscopy (2D-ES) was developed at the turn of the millennia as the optical analogue to nuclear magnetic resonance (NMR) spectroscopy.¹⁻³ Since

then, 2D-ES has become one of the most powerful and information-rich femtosecond four-wave-mixing techniques in the UV/Vis regimes. It was implemented in collinear,⁴ partially non-collinear,⁵⁻⁷ and fully non-collinear realizations^{8,9} and emerged as an efficient high-precision technique for the comprehensive real-time characterization of a large variety of material systems, from atoms¹⁰ and polyatomic chromophores¹¹ to molecular aggregates and solids.¹²⁻¹⁶

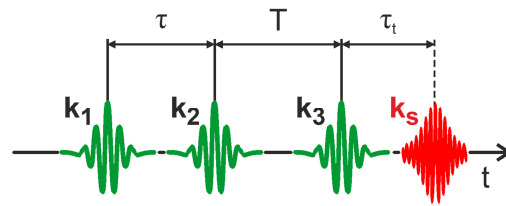
2D-ES is a variant of the third-order heterodyne-detected four-wave-mixing spectroscopy (see Figure 1(a)). The 2D-ES signal $S^{(\sigma)}(\tau, T, \tau_t)$ can be recorded in the rephasing ($\sigma = R$, $\mathbf{k}_S = \mathbf{k}_1 - \mathbf{k}_2 + \mathbf{k}_3$) or non-rephasing ($\sigma = NR$, $\mathbf{k}_S = -\mathbf{k}_1 + \mathbf{k}_2 + \mathbf{k}_3$) phase-matching direction as a function of the delay times between the first two pulses (coherence time τ), the second and the third pulses (population time T), and the last two pulses (detection time τ_t). The sketch of Figure 1(a) indicates that 2D-ES delivers four-wave-mixing signal with maximal information content as both excitation and emission frequencies are fully resolved. This allows for an unprecedented level of scrutiny of material systems, explaining why 2D-ES is so powerful and popular. 2D-ES signals are usually Fourier transformed with respect to τ (excitation frequency ω_τ) and τ_t (detection frequency ω_t), and the resultant 2D-ES spectra $S^{(\sigma)}(\omega_\tau, T, \omega_t)$ visualize how correlation between the initial (ω_τ) and final (ω_t) states of the system evolves with the population time T .

2D-ES spectra consist of three contributions, which are customarily referred to as ground-state bleach (GSB), stimulated emission (SE) and excited state absorption (ESA)

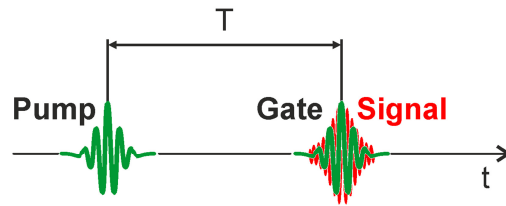
$$S^{(\sigma)}(\omega_\tau, T, \omega_t) = \sum_{j=\text{GSB, SE, ESA}} S_j^{(\sigma)}(\omega_\tau, T, \omega_t). \quad (1)$$

However, the information content of these contributions differs substantially. GSB monitors wavepacket motion on the electronic ground state, while SE and ESA reflect wavepacket dynamics on the excited electronic states. Yet, SE and ESA differ in their respective “spectator states” which are responsible for encoding the dynamical information. In the SE, the

(a) 2D electronic



(b) time-resolved FI.



(c) 2D-FLEX

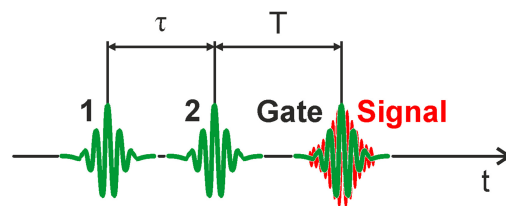


Figure 1: Pulse sequences shaping 2D-ES (a), time- and frequency-resolved fluorescence (b), and 2D-FLEX (c) signals.

wavepacket motion on the excited electronic states is projected onto the electronic ground state, while it is projected onto higher-lying excited electronic states in the ESA. For complex material systems, it is difficult to decipher the intrinsic system dynamics from GSB, SE, and notably ESA spectra. Furthermore, GSB, SE and ESA spectra usually overlap, which leads to the partial cancellation of spectral features and hinders proper interpretation of 2D-ES spectra. While the techniques of polarization-sensitive detection¹⁷⁻¹⁹ or beating maps²⁰⁻²² can partially solve the problem, they do not provide a universal solution.

As has recently been proposed by Hauer and coworkers,²³ this problem can be addressed by a novel technique, 2D fluorescence-excitation (2D-FLEX) spectroscopy, which combines the spectral resolution of excitation and detection processes inherent in 2D-ES with the exclusive detection of the SE contribution. The principle of 2D-FLEX can readily be grasped from the following considerations. Time-resolved fluorescence spectroscopy²⁴ permits a direct detection of wavepacket dynamics on the excited electronic states, but cannot provide information on electronic coherences during the excitation of the system with a single pump pulse (see Figure 1(b)). In 2D-FLEX, a single pump pulse is replaced by a pump-pulse pair delayed by a time τ , as sketched in Figure 1(c). Hence, 2D-FLEX can be envisaged as a technique combining the double-pulse excitation of 2D-ES with the broadband detection of time- and frequency-resolved fluorescence.

The high information content of 2D-FLEX spectroscopy has been demonstrated by simulating spectra for several model systems.²³ Yet, there is still a lack of practical tools to simulate 2D-FLEX spectra for realistic molecular systems. The aim of this work is to develop an *ab initio* theoretical framework for the simulation of 2D-FLEX spectra of molecular systems by interfacing the classical doorway-window representation of spectroscopic responses with trajectory surface hopping simulations. The method has been implemented for the pyrazine molecule, a system known for its multiple conical intersections of lower lying excited electronic states. The photophysics of pyrazine has been comprehensively studied by *ab initio* quantum-chemistry methods,^{25,26} dynamic calculations,^{27,28} and simulations of

nonlinear spectroscopic signals.^{29–35}

The 2D-FLEX spectra (see Figure 1(c)) can be represented as a sum of rephasing and nonrephasing contributions,

$$S_{2DF}(\omega_\tau, T, \omega_t) \sim \text{Re} \sum_{\sigma=R, NR} S_{2DF}^{(\sigma)}(\omega_\tau, T, \omega_t), \quad (2)$$

which can be further evaluated in terms of third-order response functions as follows²³

$$S_{2DF}^{(\sigma)}(\omega_\tau, T, \omega_t) \sim \int_0^\infty d\tau \int_{-\infty}^\infty dt \int_0^\infty dt_3 \int_0^\infty dt_2 \int_0^\infty dt_1 R_\sigma(t_3, t_2, t_1) e^{i\eta_\sigma \omega_\tau \tau} \times \quad (3)$$

$$e^{i\eta_\sigma \omega_{pu}(t_1 - \tau)} e^{-(\zeta - i\omega_t)t_3} E_t(t) E_t(t - t_3) E_{pu}(t + T - t_3 - t_2) E_{pu}(t + \tau + T - t_3 - t_2 - t_1).$$

Here $\sigma = R, NR$, $\eta_{NR} = 1$, $\eta_R = -1$; ω_{pu} and $E_{pu}(t)$ represent the carrier frequency and the dimensionless envelope of the pump pulse; ω_t is the fluorescence frequency, and $E_t(t)$ is the envelope of the up-conversion (gate) pulse which is responsible for the time resolution of the emitted fluorescence; t_1 , t_2 , and t_3 are the time intervals between sequential system-field interactions; $R_{NR}(t_3, t_2, t_1)$ and $R_R(t_3, t_2, t_1)$ are the non-rephasing and rephasing response functions which correspond, respectively, to the response functions $R_1(t_3, t_2, t_1)$ and $R_2(t_3, t_2, t_1)$ of Mukamel's monograph.³⁶

2D-FLEX spectra $S_{2DF}(\omega_\tau, T, \omega_t)$ of Eq. (2) and SE contributions to the total (rephasing + nonrephasing) 2D-ES spectra

$$S_{SE}(\omega_\tau, T, \omega_t) \sim \text{Re} \sum_{\sigma=R, NR} S_{SE}^{(\sigma)}(\omega_\tau, T, \omega_t), \quad (4)$$

are determined by the same response functions and are therefore quite similar. Yet, there is a fundamental difference between these two spectra.²³ The time (T) – frequency (ω_t) resolution of 2D-FLEX spectra is Fourier-limited ($\delta_T \delta_{\omega_t} \sim 1$) because it is governed by the same gate pulse (Figure 1(c)), while the time-frequency resolution of 2D-ES spectra is not

Fourier limited because it is determined by time delays between different pairs of pulses (Figure 1(a)). This observation has profound effect on the peak shapes and time-frequency resolution of 2D-FLEX and 2D-ES SE spectra. While it is instructive to compare 2D-FLEX and 2D-ES SE spectra, we note that only 2D-FLEX spectra can be measured directly. There is no experimentally feasible way to measure the SE-part of a 2D-ES spectrum.

Interfacing dynamical trajectory methods with *ab initio* electronic-structure methods into on-the-fly simulation protocols is a flourishing field of research in theoretical spectroscopy (see recent reviews³⁷⁻⁴⁴). In the context of the present work, we require a simulation protocol that can account for finite pulse durations, which, as explained above, determine the time-frequency resolution of 2D-FLEX spectra. The protocol which is based on combining trajectory surface hopping (SH) simulations^{45,46} with the classical doorway-window (DW) representation of four-wave-mixing signals excellently meets this criterion.⁴³ This protocol was developed and applied for the evaluation of transient-absorption pump-probe,²⁹ 2D-ES,³⁰ and time-resolved fluorescence spectra.⁴⁷ Its validity to predict pump-probe and 2D-ES spectra of pyrazine has recently been proved by comparing with full quantum simulations of the models of reduced dimensionality.³⁵

Since 2D-FLEX spectra combine a double-pulse excitation of 2D-ES with the detection of time- and frequency-resolved fluorescence, the DW-SH simulation protocol for 2D-FLEX spectra can be immediately constructed by combining the doorway function of 2D-ES spectra³⁰ with the window function of time-resolved fluorescence spectra.⁴⁷ The computational details are presented in Supporting Information, while the flowchart clarifying the simulation procedure is depicted in Figure 2. In the DW-SH simulation protocol, 2D-FLEX spectra can be evaluated as a product of the doorway and window functions averaged over SH trajectories

$$S_{2DF}(\omega_\tau, T, \omega_t) \sim \langle D_{2DF}(\omega_\tau, \mathbf{R}_g, \mathbf{P}_g; e) W_{2DF}(\omega_t, \mathbf{R}_e(T), \mathbf{P}_e(T); e(T)) \rangle. \quad (5)$$

Here, \mathbf{R}_g and \mathbf{P}_g are initial nuclear coordinates and momenta, which can be sampled from

the Wigner distribution in the electronic ground state, $\rho_g^{\text{Wig}}(\mathbf{R}_g, \mathbf{P}_g)$;⁴⁸ $D_{2DF}(\omega_\tau, \mathbf{R}_g, \mathbf{P}_g; e)$ is the doorway function of Eq. (S3) in the initial electronic state e sampled according to its oscillator strength and pump-frequency detuning;⁴³ $W_{2DF}(\omega_t, \mathbf{R}_e(T), \mathbf{P}_e(T); e(T))$ is the window function of Eq. (S4) in which $\mathbf{R}_e(T)$, $\mathbf{P}_e(T)$ denote nuclear positions and momenta in the electronic state $e(T)$ at the time T , and the notation $e(T)$ emphasizes that a trajectory initiated at $T=0$ fs in an excited state e may end up at time T in another excited state $e(T)$ due to nonadiabatic transitions; $\langle \dots \rangle$ denotes averaging over SH trajectories. The doorway-window expressions for the evaluation of 2D-ES SE spectra³⁰ are also presented in Supporting Information. It should be noted that the doorway and window functions are fully specified by electronic energies and transition dipole moments along SH trajectories, as well as by the carrier frequencies and envelopes of the pump and gate pulses.

In all simulations of the present work, the pump pulse is tuned into resonance with the bright state (B_{2u}) of pyrazine ($\omega_p = 5.2$ eV), and the envelopes of the pump and gate (for 2D-FLEX) and probe (for 2D-ES SE) pulses are modeled by Gaussian functions, $E_a(t) = \exp(-(t/\tau_a)^2)$, $E_a(\omega) = \exp(-(\omega\tau_a)^2/4)$, where τ_a is the pulse duration ($a = pu, t, pr$ correspond to pump, gate and probe pulse, respectively). The widths of the spectral features of 2D-FLEX and 2D-ES SE spectra are determined by the spectral widths of the laser pulses and by the peak shape broadening (see Eq. (S5)), in which the inhomogeneous broadening parameter is fixed at $\tau_\nu^{-1} = 0.05$ eV in all our calculations.

Before we delve into discussion of the simulated 2D-FLEX and 2D-ES SE spectra, it is instructive to briefly characterize the main photophysical processes in pyrazine and determine their spectroscopic manifestations. Pyrazine possesses three low-lying excited electronic states in the Franck-Condon region, the $B_{2u}(\pi\pi^*)$, $B_{3u}(n\pi^*)$ and $A_u(n\pi^*)$, which are nonadiabatically coupled through a series of conical intersections.^{25,26} The experimental gas-phase UV linear absorption spectrum of pyrazine at 353 ± 3 K is shown in Figure 3 (black, data is taken from Ref.⁴⁹). The spectrum consists of two bands, an intense band centered around 4.9 eV and a weaker band centered around 4.0 eV. These bands are attributed to the bright

B_{2u} state and the weakly absorbing B_{3u}/A_u states, respectively. It is essential that the shape and intensity of the B_{3u}/A_u band is mostly determined by the nonadiabatic coupling between the bright B_{2u} state and almost dark B_{3u}/A_u states (the so-called intensity borrowing effect). As revealed by the femtosecond photoelectron spectroscopy measurements, the $B_{2u} - B_{3u}$ coupling results in the ~ 20 fs conical-intersection-driven $B_{2u} \rightarrow B_{3u}$ population transfer.⁵⁰⁻⁵² Internal conversion from the coupled B_{2u}/B_{3u} states to the electronic ground state occurs on a much longer timescale of ~ 20 ps.⁵⁰⁻⁵² Hence, only B_{2u}/B_{3u} steady-state fluorescence of pyrazine in the gas phase was measured⁵³ and simulated.^{54,55} On the other hand, the previous simulations of time-resolved fluorescence of pyrazine in various reduced-dimensional models^{31,32,56} as well as recent *ab initio* simulations of the SE contribution to pyrazine’s transient-absorption pump-probe spectra^{29,35} reveal that the B_{2u}/B_{3u} fluorescence of pyrazine survives on a timescale of at least 150 fs, but experiences a fivefold intensity reduction caused by the B_{2u}/B_{3u} conical intersection.

Figure 4 depicts 2D-FLEX spectra $S_{2DF}(\omega_\tau, T, \omega_t)$ of pyrazine as a function of the excitation frequency ω_τ and the fluorescence frequency ω_t at population times $T = 0$ (a), 20 (b), 35 (c), 60 (d), 100 (e), 130 (f), 160 (g) and 190 fs (h). The pulse durations for the pump and gate pulses are set to $\tau_{pu} = 5$ fs (with $E_{pu}(\omega)$ plotted in red in Figure 3) and $\tau_t = 30$ fs, respectively, which corresponds to the achievable time resolution in fluorescence up-conversion experiments.^{57,58} 2D-FLEX spectra excited with longer pump pulses $\tau_{pu} = 15$ fs exhibit similar structure, but the peaks are narrower along ω_τ (see Figure S1 in Supporting Information). The spectra in Figure 4 illustrate the ability of 2D-FLEX to directly monitor the downhill (conical-intersection-mediated) population transfer. Namely, the ω_τ -position of all peaks reveals the initially excited bright B_{2u} state, while the ω_t -positions of the peaks follow the $B_{2u} \rightarrow B_{3u}$ population transfer and subsequent energy redistribution in the coupled B_{3u}/A_u states.

At $T = 0$ fs (Figure 4a), a single peak around $\omega_\tau = \omega_t = 5.2$ eV corresponds to the emission from the initially populated bright B_{2u} state. The peak is elongated along the

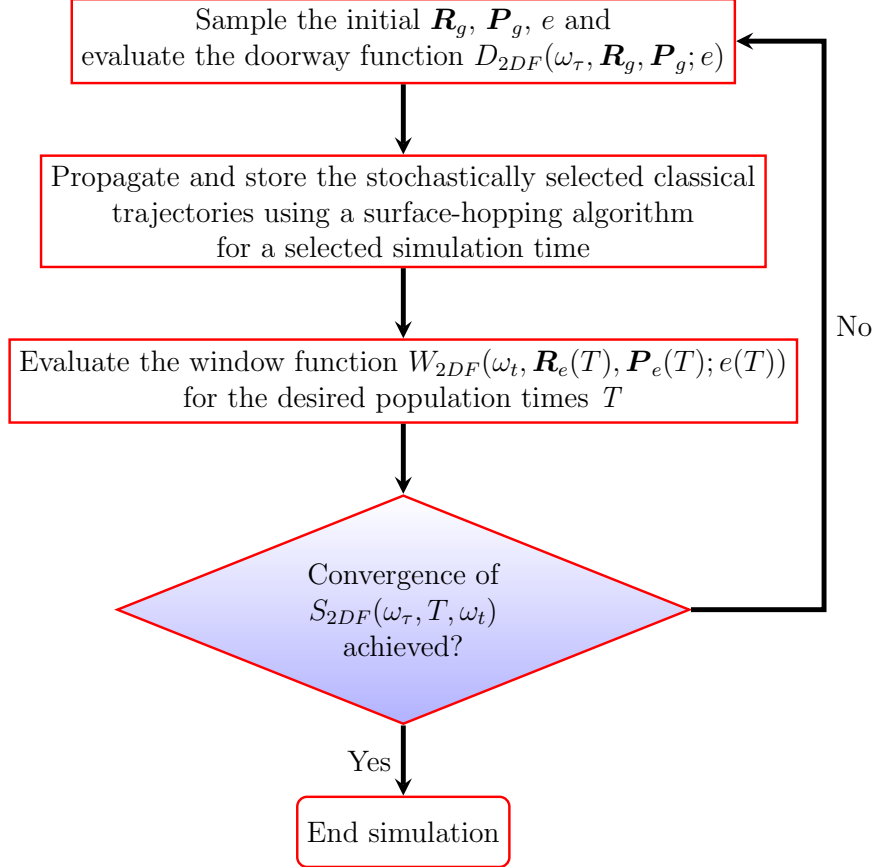


Figure 2: Flowchart depicting the simulation protocol for obtaining 2D-FLEX spectra as proposed in this work.

main diagonal, which signifies a substantial inhomogeneous broadening.⁵⁹ As T increases, the wavepacket moves down to $\omega_t \approx 4$ eV at $T = 20$ fs (Figure 4b), monitoring the conical-intersection-driven $B_{2u} \rightarrow B_{3u}$ internal conversion process. The spectrum splits into two branches at $T = 35$ fs with stronger peaks in the upper branch and weaker peaks in the lower branch (Figure 4c). At $T = 60$ fs (Figure 4d), the separation between those two branches disappears, and the spectrum exhibits pronounced doublets at $\omega_t \approx 4.4$ and 3.2 eV as well as numerous weaker peaks in the entire frequency range $2 \text{ eV} < \omega_t < 4.5 \text{ eV}$. These peaks reveal the lower vibronic levels of the B_{2u} state and higher vibronic levels of the B_{3u}/A_u states. For $T \geq 100$ fs, the spectrum splits again into upper ($\omega_t > 4.3$ eV) and lower ($\omega_t < 4$ eV) branches. At $T = 100$ fs, the upper branch is dominated by a relatively pronounced peak around $\omega_t = 4.7$ eV (Figure 4e), and the lower branch is composed of

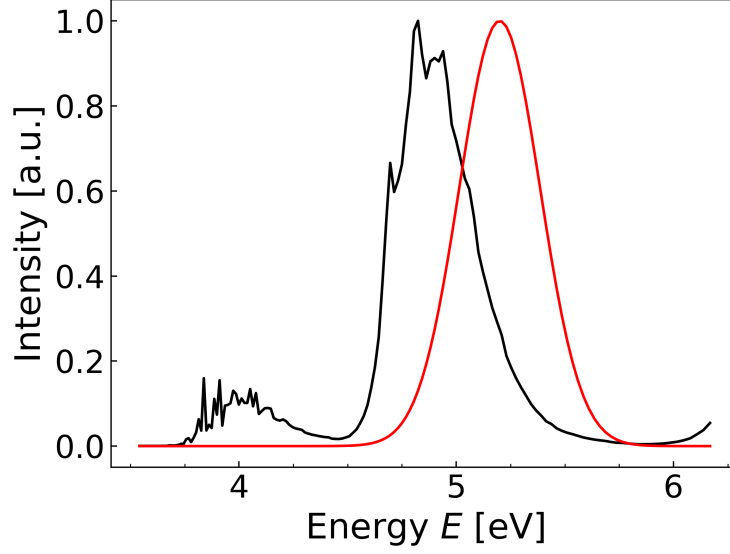


Figure 3: Black: experimental absorption spectrum of pyrazine molecule in the gas-phase at 353 ± 3 K (data is taken from Ref.⁴⁹); Red: energy profile of the Gaussian laser pulse centered at 5.2 eV with width of $\tau = 5$ fs.

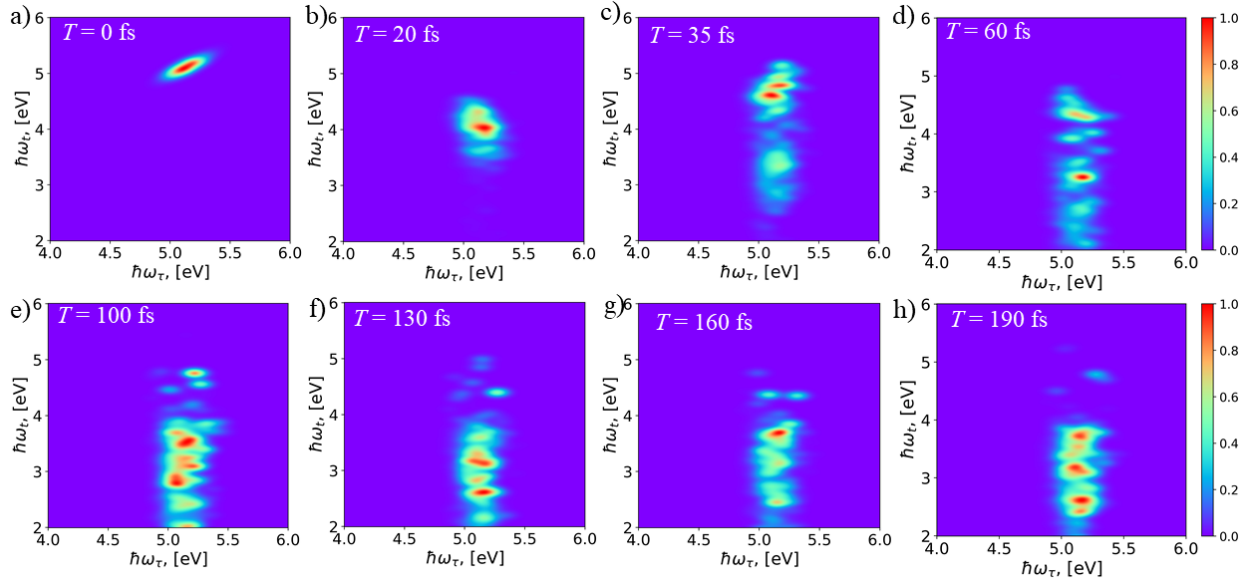


Figure 4: 2D-FLEX spectra $S_{2DF}(\omega_\tau, T, \omega_t)$ of pyrazine as a function of the excitation frequency ω_τ and the detection frequency ω_t at population times $T = 0$ (a), 20 (b), 35 (c), 60 (d), 100 (e), 130 (f), 160 (g), 190 fs (h) for $\tau_{pu} = 5$ fs and $\tau_t = 30$ fs. For each T , the intensities of the spectra are scaled for better visibility.

several well-resolved peaks in the frequency range of $\omega_t = 2.0 - 4.0$ eV which mirror the wavepacket motion in the coupled B_{3u}/A_u states. The intensities of peaks in both upper and lower branches decrease with T , indicating the irreversible $B_{2u} \rightarrow B_{3u}/A_u$ population transfer (see Figures 4e-h). From $T = 0$ fs to $T = 190$ fs, the maximum intensities of the 2D-FLEX spectra decrease by a factor of about 36. The complete time evolution of 2D-FLEX spectra with a time step of 5 fs for T are shown in Figures S2-S6 in the Supporting Information.

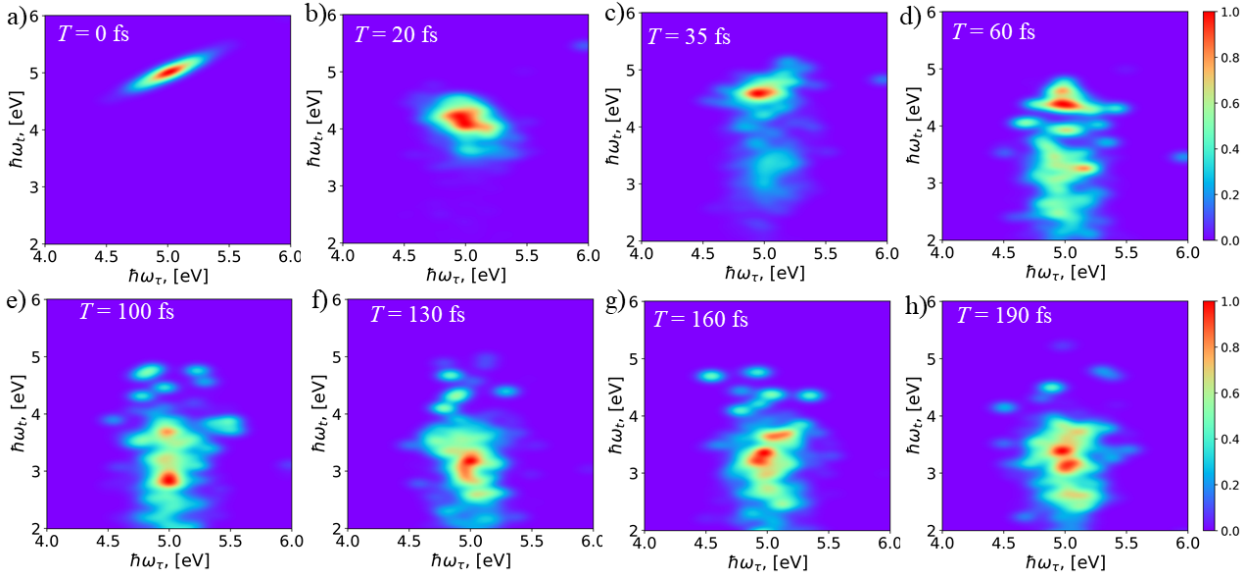


Figure 5: 2D-ES SE spectra $S_{SE}(\omega_\tau, T, \omega_t)$ of pyrazine as a function of the excitation frequency ω_τ and the detection frequency ω_t at population times $T = 0$ (a), 20 (b), 35 (c), 60 (d), 100 (e), 130 (f), 160 (g), 190 fs (h) for $\tau_{pu} = \tau_{pr} = 0.1$ fs. For each T , the intensities of the spectra are scaled for better visibility.

The 2D-ES SE spectra simulated with pulse durations of $\tau_{pu} = \tau_{pr} = 5$ fs at different population times T monitor exclusively the time evolution of a single peak around $\omega_\tau = \omega_t = 5.2$ eV, while the peaks for lower ω_t completely vanish (see Figure S7 in the Supporting Information). This is because the laser pulse with duration of $\tau = 5$ fs only covers the B_{2u} band of absorption spectrum of pyrazine, but does not overlap with the B_{3u}/A_u band (see the energy profile of the laser pulse in Figure 3). To cover the entire frequency domain of the absorption spectrum of pyrazine, one needs to use nowadays unavailable attosecond pulses.

The 2D-ES SE spectra simulated with such pulses ($\tau_{pu} = \tau_{pr} = 0.1$ fs, almost impulsive limit) at population times $T = 0$ (a), 20 (b), 35 (c), 60 (d), 100 (e), 130 (f), 160 (g), 190 fs (h) are displayed in Figure 5. Comparison of Figures 4 and 5 shows that positions of the peaks of 2D-ES SE and 2D-FLEX spectra coincide, as expected. Furthermore, intensities of the peaks in 2D-ES SE spectra decrease by a factor of 44 from $T = 0$ to $T = 190$ fs, which is only slightly larger than a factor of 36 for 2D-FLEX spectra. However, different detection schemes affect significantly the spectral resolution and peak shapes of the two signals. While 2D-FLEX spectra in Figure 4 exhibit distinct peaks along ω_t , the peaks of 2D-ES SE spectra in Figure 5 are much broader. The reason for this difference is as follows. The widths of peaks of 2D-ES SE spectra in Figure 5 are primarily determined by the optical dephasing parameter of 0.05 eV and are almost independent of the spectral widths of the laser pulses (impulsive limit). The widths and shapes of peaks of 2D-FLEX spectra in Figure 4 are predominantly determined by the spectral widths of the pump and gate pulses.

Comparison of simulated 2D-FLEX and 2D-ES SE spectra demonstrates that different detection schemes can affect the signal dramatically. Detection of 2D-ES SE spectra is determined by the carrier frequencies and bandwidths of the pulses (cf. Ref.⁶⁰). As a result, obtaining 2D-ES SE spectra of pyrazine in the entire energy domain of $2 \text{ eV} \leq \omega_t \leq 5.2 \text{ eV}$ requires attosecond pulses. On the other hand, detection of 2D-FLEX spectra in a broad range of wavelengths of spontaneously emitted photons allows fine-tuning of the simultaneous time- and frequency-resolution,^{61,62} which in turn yields a highly informative and detailed view of the intramolecular energy transfer and redistribution. Hence, 2D-FLEX can become a method of choice for studying complex nonadiabatic dynamics which could only be monitored by 2D-ES with still unavailable attosecond pulses.

In summary, we develop an on-the-fly SH protocol for the simulation of 2D-FLEX spectra of polyatomic chromophores. If necessary, the developed simulation routine can be further enhanced by employing the machine-learning technique following the recipes of Ref.³⁵. The simulated 2D-FLEX spectra of pyrazine demonstrate that three facets ensure high predictive

power and information content of this novel spectroscopic technique. (i) Similar to 2D-ES, 2D-FLEX spectra monitor wavepacket motions of molecular systems excited at frequency ω_τ and probed at frequency ω_t . (ii) In contrast to 2D-ES, 2D-FLEX spectra contain exclusively the SE contribution. (iii) 2D-FLEX spectra provide sufficient temporal and spectral resolution by employing the experimentally available pump ($\tau_{pu} \sim 5$ fs) and gate ($\tau_t \sim 30$ fs) pulses, as well as cover the spectral range of several eV along ω_t . Separately, the facets (i)-(iii) are inherent in a number of spectroscopic techniques. For example, time-resolved fluorescence detects solely SE contribution with sufficient temporal (T) and frequency (ω_t) resolution,^{57,58} and UV/Vis 2D-ES SE spectra permit broadband detection.^{6,63} It is the combination of all three facets that makes 2D-FLEX spectroscopy a highly promising tool for scrutinizing nonadiabatic dynamics in a number of molecular systems. It is expected that the present work will promote practical implementation of 2D-FLEX spectroscopy and facilitate interpretation of the forthcoming 2D-FLEX experiments.

Supporting Information

Doorway-Window functions in 2D-FLEX, Computational details, 2D-FLEX spectra for $\tau_{pu} = 15$ fs, the complete time evolution of 2D-FLEX spectra for $\tau_{pu} = 5$ fs, 2D-ES SE spectra for $\tau_{pu} = \tau_{pr} = 5$ fs.

Acknowledgement

S.V.P. and L.P.C. acknowledge support from the starting grant of research center of new materials computing of Zhejiang Lab (No. 3700-32601). M.F.G. acknowledges support from the National Natural Science Foundation of China (No. 22373028). L.V. acknowledges postdoctoral fellowship of Hangzhou Dianzi University. J.H. acknowledges support from the Deutsche Forschungsgemeinschaft (DFG, German Research Foundation), Project No. 514636421.

Data availability statement

The data is available from the authors upon reasonable request.

Code availability statement

The code for the generation of 2D-FLEX spectra from *ab initio* data is available at https://github.com/psebastianzjl/2d_flex_spectra_generation.

Competing interests

The authors declare that they have no competing interests.

References

- (1) Jonas, D. M. Optical Analogs of 2D NMR. *Science*. **2003**, *300*, 1515–1517.
- (2) Tian, P.; Keusters, D.; Suzuki, Y.; Warren, W. S. Femtosecond Phase-Coherent Two-Dimensional Spectroscopy. *Science*. **2003**, *300*, 1553–1555.
- (3) Hochstrasser, R. M. Two-dimensional spectroscopy at infrared and optical frequencies. *Proc. Natl. Acad. Sci. U. S. A.* **2007**, *104*, 14190–14196.
- (4) Wagner, W.; Li, C.; Semmlow, J.; Warren, W. S. Rapid phase-cycled two-dimensional optical spectroscopy in fluorescence and transmission mode. *Opt. Express* **2005**, *13*, 3697–3706.
- (5) DeFlores, L. P.; Nicodemus, R. A.; Tokmakoff, A. Two-dimensional Fourier transform spectroscopy in the pump-probe geometry. *Opt. Lett.* **2007**, *32*, 2966–2968.

- (6) Krebs, N.; Pugliesi, I.; Hauer, J.; Riedle, E. Two-Dimensional Fourier Transform Spectroscopy in the Ultraviolet with sub-20 fs Pump Pulses and 250-720 nm Supercontinuum Probe. *New J. Phys.* **2013**, *15*, 085016.
- (7) Fuller, F. D.; Ogilvie, J. P. Experimental implementations of two-dimensional Fourier transform electronic spectroscopy. *Annu. Rev. Phys. Chem.* **2015**, *66*, 667–690.
- (8) Brixner, T.; Mančal, T.; Stiopkin, I. V.; Fleming, G. R. Phase-stabilized two-dimensional electronic spectroscopy. *J. Chem. Phys.* **2004**, *121*, 4221–4236.
- (9) Milota, F.; Lincoln, C. N.; Hauer, J. Precise phasing of 2D-electronic spectra in a fully non-collinear phase-matching geometry. *Opt. Express* **2013**, *21*, 15904–15911.
- (10) Uhl, D.; Bangert, U.; Bruder, L.; Stienkemeier, F. Coherent optical 2D photoelectron spectroscopy. *Optica* **2021**, *8*, 1316–1324.
- (11) Mewes, L.; Ingle, R. A.; Al Haddad, A.; Chergui, M. Broadband visible two-dimensional spectroscopy of molecular dyes. *J. Chem. Phys.* **2021**, *155*, 034201.
- (12) Brixner, T.; Stenger, J.; Vaswani, H. M.; Cho, M.; Blankenship, R. E.; Fleming, G. R. Two-Dimensional Spectroscopy of Electronic Couplings in Photosynthesis. *Nature*. **2005**, *434*, 625–628.
- (13) Engel, G. S.; Calhoun, T. R.; Read, E. L.; Ahn, T.-K.; Mančal, T.; Cheng, Y.-C.; Blankenship, R. E.; Fleming, G. R. Evidence for wavelike energy transfer through quantum coherence in photosynthetic systems. *Nature*. **2007**, *446*, 782–786.
- (14) Lim, J.; Paleček, D.; Caycedo-Soler, F.; Lincoln, C. N.; Prior, J.; Von Berlepsch, H.; Huelga, S. F.; Plenio, M. B.; Zigmantas, D.; Hauer, J. Vibronic origin of long-lived coherence in an artificial molecular light harvester. *Nat. Commun.* **2015**, *6*, 7755.
- (15) Collini, E. 2D electronic spectroscopic techniques for quantum technology applications. *J. Phys. Chem. C* **2021**, *125*, 13096–13108.

- (16) Biswas, S.; Kim, J.; Zhang, X.; Scholes, G. D. Coherent two-dimensional and broadband electronic spectroscopies. *Chem. Rev.* **2022**, *122*, 4257–4321.
- (17) Hochstrasser, R. M. Two-dimensional IR-spectroscopy: polarization anisotropy effects. *Chem. Phys.* **2001**, *266*, 273–284.
- (18) Gelin, M. F.; Domcke, W. Simple recipes for separating excited-state absorption and cascading signals by polarization-sensitive measurements. *J. Phys. Chem. A* **2013**, *117*, 11509–11513.
- (19) Farrell, K. M.; Yang, N.; Zanni, M. T. A polarization scheme that resolves cross-peaks with transient absorption and eliminates diagonal peaks in 2D spectroscopy. *Proc. Natl. Acad. Sci. U. S. A.* **2022**, *119*, e2117398119.
- (20) Fuller, F. D.; Pan, J.; Gelzinis, A.; Butkus, V.; Senlik, S. S.; Wilcox, D. E.; Yocum, C. F.; Valkunas, L.; Abramavicius, D.; Ogilvie, J. P. Vibronic coherence in oxygenic photosynthesis. *Nat. Chem.* **2014**, *6*, 706–711.
- (21) Thyryhaug, E.; Tempelaar, R.; Alcocer, M. J. P.; Židek, K.; Bina, D.; Knoester, J.; Jansen, T. L. C.; Zigmantas, D. Identification and Characterization of Diverse Coherences in the Fenna–Matthews–Olson Complex. *Nat. Chem.* **2018**, *10*, 780–786.
- (22) Duan, H. G.; Jha, A.; Chen, L.; Tiwari, V.; Cogdell, R. J.; Ashraf, K.; Prokhorenko, V. I.; Thorwart, M.; Miller, R. J. D. Quantum Coherent Energy Transport in the Fenna–Matthews–Olson Complex at Low Temperature. *Proc. Natl. Acad. Sci. U. S. A.* **2022**, *119*, e2212630119.
- (23) Yang, J.; Gelin, M. F.; Chen, L.; Šanda, F.; Thyryhaug, E.; Hauer, J. Two-dimensional fluorescence excitation spectroscopy: A novel technique for monitoring excited-state photophysics of molecular species with high time and frequency resolution. *J. Chem. Phys.* **2023**, *159*, 074201.

- (24) Kumpulainen, T.; Lang, B.; Rosspeintner, A.; Vauthey, E. Ultrafast Elementary Photochemical Processes of Organic Molecules in Liquid Solution. *Chem. Rev.* **2017**, *117*, 10826–10939.
- (25) Woywod, C.; Domcke, W.; Sobolewski, A. L.; Werner, H.-J. Characterization of the S₁–S₂ Conical Intersection in Pyrazine Using *ab initio* Multiconfiguration Self-Consistent-Field and Multireference Configuration-Interaction Methods. *J. Chem. Phys.* **1994**, *100*, 1400–1413.
- (26) Sala, M.; Lasorne, B.; Gatti, F.; Guérin, S. The Role of the Low-lying Dark nπ* States in the Photophysics of Pyrazine: a Quantum Dynamics Study. *Phys. Chem. Chem. Phys.* **2014**, *16*, 15957–15967.
- (27) Xie, W.; Sapunar, M.; Došlić, N.; Sala, M.; Domcke, W. Assessing the Performance of Trajectory Surface Hopping Methods: Ultrafast Internal Conversion in Pyrazine. *J. Chem. Phys.* **2019**, *150*, 154119.
- (28) Chen, L.; Gelin, M. F.; Domcke, W. Multimode Quantum Dynamics with Multiple Davydov D2 Trial States: Application to a 24-Dimensional Conical Intersection Model. *J. Chem. Phys.* **2019**, *150*, 024101.
- (29) Gelin, M. F.; Huang, X.; Xie, W.; Chen, L.; Došlić, N.; Domcke, W. Ab Initio Surface-Hopping Simulation of Femtosecond Transient-Absorption Pump–Probe Signals of Nonadiabatic Excited-State Dynamics Using the Doorway–Window Representation. *J. Chem. Theory Comput.* **2021**, *17*, 2394–2408.
- (30) Huang, X.; Xie, W.; Došlić, N.; Gelin, M. F.; Domcke, W. Ab Initio Quasiclassical Simulation of Femtosecond Time-Resolved Two-Dimensional Electronic Spectra of Pyrazine. *J. Phys. Chem. Lett.* **2021**, *12*, 11736–11744.
- (31) Sun, K.; Xie, W.; Chen, L.; Domcke, W.; Gelin, M. F. Multi-Faceted Spectroscopic

- Mapping of Ultrafast Nonadiabatic Dynamics near Conical Intersections: A Computational Study. *J. Chem. Phys.* **2020**, *153*, 174111.
- (32) Chen, L.; Sun, K.; Shalashilin, D. V.; Gelin, M. F.; Zhao, Y. Efficient Simulation of Time- and Frequency-Resolved Four-Wave-Mixing Signals with a Multiconfigurational Ehrenfest Approach. *J. Chem. Phys.* **2021**, *154*, 054105.
- (33) Piteša, T.; Sapunar, M.; Ponzi, A.; Gelin, M. F.; Došlić, N.; Domcke, W.; Decleva, P. Combined Surface-Hopping, Dyson Orbital, and B-Spline Approach for the Computation of Time-Resolved Photoelectron Spectroscopy Signals: The Internal Conversion in Pyrazine. *J. Chem. Theory Comput.* **2021**, *17*, 5098–5109.
- (34) Kaczun, T.; Dempwolff, A. L.; Huang, X.; Gelin, M. F.; Domcke, W.; Dreuw, A. Tuning UV Pump X-ray Probe Spectroscopy on the Nitrogen K Edge Reveals the Radiationless Relaxation of Pyrazine: Ab Initio Simulations Using the Quasiclassical Doorway–Window Approximation. *J. Phys. Chem. Lett.* **2023**, *14*, 5648–5656.
- (35) Pios, S. V.; Gelin, M. F.; Ullah, A.; Dral, P. O.; Chen, L. Artificial-Intelligence-Enhanced On-the-Fly Simulation of Nonlinear Time-Resolved Spectra. *J. Phys. Chem. Lett.* **2024**, *15*, 2325–2331.
- (36) Mukamel, S. *Principles of nonlinear optical spectroscopy*; Oxford University Press, 1995.
- (37) Vaníček, J. Several Semiclassical Approaches to Time-resolved Spectroscopy. *CHIMIA* **2017**, *71*, 283–287.
- (38) Segarra-Martí, J.; Mukamel, S.; Garavelli, M.; Nenov, A.; Rivalta, I. Towards Accurate Simulation of Two-Dimensional Electronic Spectroscopy. *Top. Curr. Chem.* **2018**, *376*, 24.
- (39) Conti, I.; Cerullo, G.; Nenov, A.; Garavelli, M. Ultrafast Spectroscopy of Photoactive

- Molecular Systems from First Principles: Where We Stand Today and Where We Are Going. *J. Am. Chem. Soc.* **2020**, *142*, 16117–16139.
- (40) Jansen, T. L. C. Computational Spectroscopy of Complex Systems. *J. Chem. Phys.* **2021**, *155*, 170901.
- (41) Zuehlsdorff, T. J.; Shedge, S. V.; Lu, S.; Hong, H.; Aguirre, V. P.; Shi, L.; Isborn, C. M. Vibronic and Environmental Effects in Simulations of Optical Spectroscopy. *Annu. Rev. Phys. Chem.* **2021**, *72*, 165–188.
- (42) Santoro, F.; Green, J. A.; Martinez-Fernandez, L.; Cerezo, J.; Improta, R. Quantum and Semiclassical Dynamical Studies of Nonadiabatic Processes in Solution: Achievements and Perspectives. *Phys. Chem. Chem. Phys.* **2021**, *23*, 8181–8199.
- (43) Gelin, M. F.; Chen, L.; Domcke, W. Equation-of-Motion Methods for the Calculation of Femtosecond Time-Resolved 4-Wave-Mixing and N-Wave-Mixing Signals. *Chem. Rev.* **2022**, *122*, 17339–17396.
- (44) Krumland, J.; Guerrini, M.; De Sio, A.; Lienau, C.; Cocchi, C. Two-dimensional electronic spectroscopy from first principles. *Appl. Phys. Rev.* **2024**, *11*, 011305.
- (45) Tully, J. C. Molecular Dynamics with Electronic Transitions. *J. Chem. Phys.* **1990**, *93*, 1061–1071.
- (46) Crespo-Otero, R.; Barbatti, M. Recent Advances and Perspectives on Nonadiabatic Mixed Quantum–Classical Dynamics. *Chem. Rev.* **2018**, *118*, 7026–7068.
- (47) Xu, C.; Lin, C.; Peng, J.; Zhang, J.; Lin, S.; Gu, F. L.; Gelin, M. F.; Lan, Z. On-the-fly simulation of time-resolved fluorescence spectra and anisotropy. *J. Chem. Phys.* **2024**, *160*, 104109.
- (48) Hillery, M.; O’Connell, R. F.; Scully, M. O.; Wigner, E. P. Distribution Functions in Physics: Fundamentals. *Phys. Rep.* **1984**, *106*, 121–167.

- (49) Samir, B.; Kalalian, C.; Roth, E.; Salghi, R.; Chakir, A. Gas-phase UV absorption spectra of pyrazine, pyrimidine and pyridazine. *Chem. Phys. Lett.* **2020**, *751*, 137469.
- (50) Stert, V.; Farmanara, P.; Radloff, W. Electron Configuration Changes in Excited Pyrazine Molecules Analyzed by Femtosecond Time-Resolved Photoelectron Spectroscopy. *J. Chem. Phys.* **2000**, *112*, 4460–4464.
- (51) Suzuki, Y. I.; Fuji, T.; Horio, T.; Suzuki, T. Time-Resolved Photoelectron Imaging of Ultrafast $S_2 \rightarrow S_1$ Internal Conversion through Conical Intersection in Pyrazine. *J. Chem. Phys.* **2010**, *132*, 174302.
- (52) Horio, T.; Spesyvtsev, R.; Nagashima, K.; Ingle, R. A.; Suzuki, Y. I.; Suzuki, T. Full Observation of Ultrafast Cascaded Radiationless Transitions from S_2 ($\pi\pi^*$) State of Pyrazine using Vacuum Ultraviolet Photoelectron Imaging. *J. Chem. Phys.* **2016**, *145*, 044306.
- (53) Kommandeur, J.; Majewski, W. A.; Meerts, W. L.; Pratt, D. W. Pyrazine: An “Exact” Solution to the Problem of Radiationless Transitions. *Ann. Rev. Phys. Chem.* **1987**, *38*, 433–462.
- (54) Stock, G.; Domcke, W. Theory of resonance Raman scattering and fluorescence from strongly vibronically coupled excited states of polyatomic molecules. *J. Chem. Phys.* **1990**, *93*, 5496–5509.
- (55) Seidner, L.; Stock, G.; Sobolewski, A.; Domcke, W. Ab initio characterization of the S_1 – S_2 conical intersection in pyrazine and calculation of spectra. *J. Chem. Phys.* **1992**, *96*, 5298–5309.
- (56) Chen, L.; Gelin, M. F.; Zhao, Y.; Domcke, W. Mapping of Wave Packet Dynamics at Conical Intersections by Time- and Frequency-Resolved Fluorescence Spectroscopy: A Computational Study. *J. Phys. Chem. Lett.* **2019**, *10*, 5873–5880.

- (57) Rhee, H.; Joo, T. Noncollinear phase matching in fluorescence upconversion. *Opt. Lett.* **2005**, *30*, 96–98.
- (58) Kim, C. H.; Joo, T. Ultrafast time-resolved fluorescence by two photon absorption excitation. *Opt. Express* **2008**, *16*, 20742–20747.
- (59) Zhan, S.; Gelin, M. F.; Huang, X.; Sun, K. Ab initio simulation of peak evolutions and beating maps for electronic two-dimensional signals of a polyatomic chromophore. *J. Chem. Phys.* **2023**, *158*, 194106.
- (60) de A. Camargo, F. V.; Grimmelsmann, L.; Anderson, H. L.; Meech, S. R.; Heisler, I. A. Resolving Vibrational from Electronic Coherences in Two-Dimensional Electronic Spectroscopy: The Role of the Laser Spectrum. *Phys. Rev. Lett.* **2017**, *118*, 033001.
- (61) Mukamel, S.; Ciordas-Ciurdariu, C.; Khidekel, V. Time-Frequency and Coordinate-Momentum Wigner Wavepackets in Nonlinear Spectroscopy. *Adv. Chem. Phys.* **1997**, *101*, 345–372.
- (62) Egorova, D.; Gelin, M. F.; Domcke, W. Time- and frequency-resolved fluorescence spectra of nonadiabatic dissipative systems: What photons can tell us. *J. Chem. Phys.* **2005**, *122*, 134504.
- (63) Timmer, D.; Lünemann, D. C.; Riese, S.; Sio, A. D.; Lienau, C. Full visible range two-dimensional electronic spectroscopy with high time resolution. *Opt. Express* **2024**, *32*, 835–847.